International Journal of Modern Physics A
Vol. 34 (2019) 1942019 (15 pages)

DOI: 10.1142/S0217751X19420193

Application of nature-inspired optimization algorithms and machine learning for heavy-ion synchrotrons

Sabrina Appel*, Wolfgang Geithner†, Stephan Reimann‡,
Mariusz Sapinski§ and Rahul Singh¶

GSI Helmoltzzentrum für Schwerionenforschung GmbH,
Darmstadt, Germany
**s.appel@gsi.de*
†*w.geithner@gsi.de*
‡*s.reimann@gsi.de*
§*m.sapinski@gsi.de*
¶*r.singh@gsi.de*

Dominik Vilsmeier

Johann Wolfgang Goethe-University Frankfurt,
Frankfurt am Main, Germany
d.vilsmeier@gsi.de

Received 28 February 2019
Revised 8 May 2019
Accepted 24 May 2019
Published 11 December 2019

The application of machine learning and nature-inspired optimization methods, like for example genetic algorithms (GA) and particle swarm optimization (PSO) can be found in various scientific/technical areas. In recent years, these approaches are finding application in accelerator physics to a greater extent. In this paper, nature-inspired optimization as well as the machine learning will be shortly introduced and their application to the accelerator facility at GSI/FAIR will be presented. For the heavy-ion synchrotron SIS18 at GSI, the multi-objective GA/PSO optimization resulted in a significant improvement of multi-turn injection performance and subsequent transmission for intense beams. An automated injection optimization with genetic algorithms at the CRYRING@ESR ion storage ring has been performed. The usage of machine learning for a beam diagnostic application, where reconstruction of space-charge distorted beam profiles from ionization profile monitors is performed, will also be shown. First results and the experience gained will be presented.

Keywords: Automated optimization; nature-inspired optimization methods; machine learning; signal reconstruction.

PACS numbers: 29.20.db, 29.27.Ac

*Corresponding author.

1. Introduction

The Facility for Antiproton and Ion Research (FAIR) will provide antiproton and ion beams of unprecedented intensities as well as qualities to drive forefront heavy ion and antimatter research.[1] The multi-turn injection (MTI) into heavy-ion synchrotron SIS18 is one of the bottlenecks for providing designed intensities for FAIR operation. The loss-induced vacuum degradation and associated lifetime reduction for intermediate charge state ions is one of the key intensity limiting factors for SIS18.[2] Beam loss during injection can trigger the pressure bump instability. An optimized injection can relax the dynamic vacuum problem, but is also crucial to reach the synchrotron intensity limit by a large multiplication of the injected current.[3]

The complexity of the FAIR facility demands a high level of automation to keep anticipated manpower requirements within acceptable levels.[4] An example of complexity is the High Energy Beam Transport System of FAIR which forms a complex system connecting among other things seven storage rings and experiment caves and has a total length of 2350 meters.[5] An automatized machine based optimization would improve the time for optimization and control of HEBT.

In the frame of the Swedish in-kind contribution to the FAIR project, the storage ring CRYRING@ESR is planned to be used for experiments with low-energy ions and protons. Figure 1 shows the CRYRING@ESR and is local injector. Over the second transfer line the CRYRING@ESR can also receive beams form the experimental storage ring ESR. The ring is already installed in the existing GSI target hall and commissioning has started in 2015.[6–8] Since CRYRING@ESR has its own local injector, it can be used as stand-alone for testing novel technical developments like automatized configuration of beam line devices. A semi-automatized optimization has been already preformed at the CRYRING in Sweden.[9]

For the optimization and control of synchrotrons, the knowledge of beam parameters is a key ingredient. Ionization profile monitors play an important role in nondestructive measurements of the transverse beam profile. They make use of

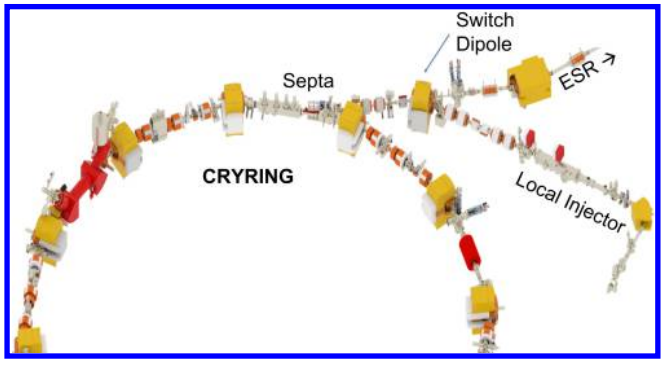

Fig. 1. CRYRING@ESR injection from the local injector has been online optimized with an evolutionary algorithm.

residual gas ionization by the particle beam and collect the ionization products via appropriate guiding fields. However, for the foreseen intensities at heavy-ion synchrotron SIS100 for some beams, a profile distortion is expected to be visible. Here, the application of machine learning allows the reconstruction of the beam profiles with simulation supported training.

2. Nature-Inspired Optimization

Nature-inspired optimization algorithms often perform well approximating solutions to all types of problems because they ideally do not make any assumption about the underlying fitness landscape. The *fitness* determines the quality of the solution and determines the probability of its survival for the next optimization step. The fitness is evaluated by an objective function, a simulation code or a real running system. In many real-life problems, multi-quantities have to be optimized. In addition, these quantities can be contradicting and there is more than one equally valid solution. These solutions form a so-called Pareto front (PA front) in the solution space, see Fig. 2.[10] A solution is Pareto optimal if it is not dominated by any other solution. By using a nondominated selection algorithm, one tries to find solutions near the optimal Pareto set.

2.1. *Evolutionary algorithms*

An evolutionary algorithm (EA) is inspired by biological evolution, such as *reproduction*, *mutation*, *recombination*, and *selection*. Genetic algorithms (GA) is the most popular type of EA. In GA terminology, a solution vector is called an *individual* and represents a set of variables; one variable is a *gene*. A group of individuals form a *population*, the following child populations are counted in *generations*. The first population is created randomly. The *crossover* operator exchanges variables

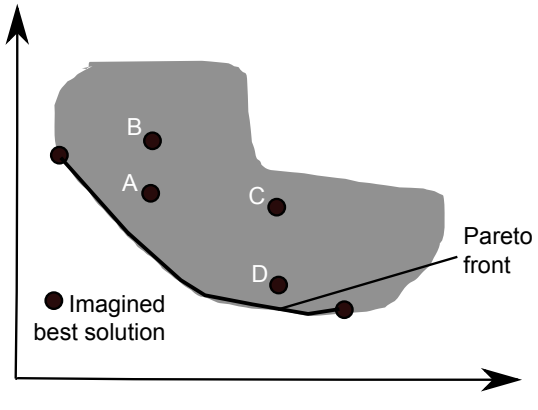

Fig. 2. The Pareto front in the solution space. The solutions A and D are located near the Pareto front and are nondominated, while solutions B and C are either dominated by solutions A or D. The solutions B and C do not dominate.

between two individuals — the parents — to discover with their offspring promising areas in the solution space (*exploration*). For the optimization within a promising area, the mutation operator changes randomly the characteristics of individuals on the gene level (*exploitation*). Reproduction of individuals for the next generation involves selection. During optimization, the most promising individuals are chosen to create the next generation. By allowing individuals with poor fitness to take part in the creation process the population is prevented to be dominated by a single individual. The most popular techniques for a single-objective optimization are proportional selection, ranking and tournament selection.[10,11]

For a multi-objective genetic optimization, there are many different algorithms available. One of them is the $(\mu + \lambda)$-algorithms. In the $(\mu + \lambda)$-algorithms as first step the individual fitness of μ-individuals are evaluated. μ is the population size and λ the offsprings size. Second, the evolutionary loop begins by producing $\lambda < \mu$-offsprings from the population through crossover and mutation. The offsprings are then evaluated and the next generations population is selected from both the offspring's and the current population. Finally, when a given number of generations has been evaluated, the algorithm returns the final population including the best solution.[13]

2.2. *Particle swarm optimization*

The initial inspiration for the Particle Swarm Optimization (PSO) came from the "graceful but unpredictable choreography of a bird flock" and is an example of alternative algorithms. The key to the swarm success lies in *social influence* and *learning*. Each individual's behavior is influenced by its own *personal experience* and the *social standard*.[11] Within a swarm, each individual refers to a point in the variable space x_i. It is updated by adding a velocity v_i depending on the personal experience C_1 and the socially swarm influence C_2. The "nostalgia" in the individual tends to return to a place it encountered in the past that best fulfilled the objectives reflected by the personal best P_i^l. Simultaneously, the individuals seek to attain publicized knowledge or social norms, reflected by the best position ever for the entire swarm P^g. The movements of the swarm are guided by improved positions, which are updated during the optimization over:

$$x_i(t+1) = x_i(t) + v_i(t+1)\,, \tag{1a}$$

$$v_i(t+1) = wv_i(t) + r_1C_1\big(P_i^l - x_i\big) + r_2C_2(P^g - x_i)\,. \tag{1b}$$

Including in addition stochastic elements r_1, r_2 in the algorithm allows to search widely and hopefully finding a satisfactory solution. PSO has shown faster convergence than GA optimization.[11]

3. Injection Optimization

SIS18 (Fig. 3) will serve as a booster for SIS100 in the FAIR facility to provide ion beams of unprecedented intensities and qualities. An optimized interface between

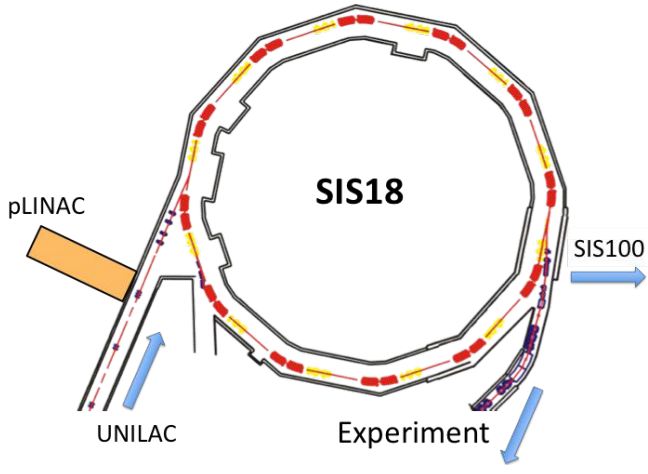

Fig. 3. The heavy-ion synchrotron SIS18 and its injectors.

injector linacs and synchrotron is mandatory to achieve high intensities. The new FAIR proton linac (pLINAC) will provide the high intensity primary proton beam for the production of antiprotons. The existing GSI heavy ion linac (UNILAC) is able to deliver world record uranium ion beam intensities for injection into the SIS18, but it is not suitable for FAIR operation. Therefore, an upgrade program is planned to replace the post-stripper section.[12] An evolutionary algorithm-based optimization of the multi-turn injection (MTI) of the SIS18 has been performed to define the interface parameters for UNILAC and pLINAC. The goal of the optimization is to stack the beamlets injected from the injector in the horizontal phase space until the synchrotron intensity limit is reached. Thereby, injection losses on the septum or acceptance have to be minimized to prevent a synchrotron performance reduction to due loss induced vacuum degradation.[3] If η characterizes the ratio between lost and injected particles, the gain factor (e.g. multiplication factor of the injected current) follows to

$$m = n(1 - \eta)\,, \tag{2}$$

where n is the ratio between injection and revolution time. For loss-free injection η is zero and the gain factor m is equal to the number of injected turns n.

However, the required MTI brilliance should be in a reachable value frame for the injector linac. As MTI has to fulfill Liouville's theorem, four bumper magnets create a time variable closed orbit bump such that the injection septum deflects the next incoming beamlet into available horizontal phase space close to the formerly injected beamlets. For effective adaptation to the free phase space, for instance, an exponential bump reduction can be chosen.

During the nature-inspired optimization, the parameters on which the MTI depends are altered in consideration of the limitations in technical and physical

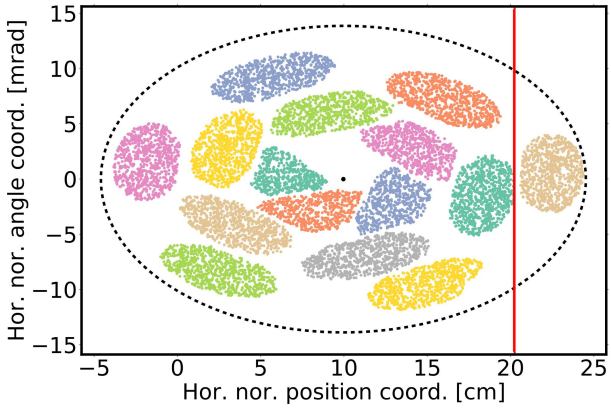

Fig. 4. Snapshot of a MTI simulation with loss. The vertical line indicates the septum and dashed line the acceptance.

conditions to find an excellent MTI performance:

$$\begin{cases} \text{minimize } \eta(n, \epsilon_x, I_0, x_c, x'_c, M, x, x', \tau, Q_x)\,, \\ \text{maximize } m(n, \epsilon_x, I_0, x_c, x'_c, M, x, x', \tau, Q_x)\,, \\ \text{maximize } \epsilon_x(n, \epsilon_x, I_0, x_c, x'_c, M, x, x', \tau, Q_x)\,. \end{cases} \tag{3}$$

The MTI performance depends on injector emittance ϵ_x and current I_0, position x and angular of the incoming beam x', the closed orbit at the septum x_c, x'_c, horizontal tune Q_x, miss-match of the incoming beam M and the orbit bump reduction τ. This parameter has been varied by evolutionary algorithms to find a injection with low loss, large gain factor and large emittance.

For the optimization the Distributed Evolutionary Algorithms in Python (DEAP)[13] together with tracking code pyORBIT — the Python implementation of ORBIT (Objective Ring Beam Injection and Tracking) code — has been used. The SIS18 MTI model has been implemented in pyORBIT and was carefully validated against experiments.[14–16] Figure 4 shows a snapshot of a MTI simulation with loss in normalized coordinates. The loss areas — inner and outside of the septum as well as the acceptance — are visible. The inner beamlets lost particles at septum earlier during the injection process and therefore not overlap. The injected beams are spirally arranged. The first injected beams are sitting in the center of the spiral next due to the closed orbit indicated by the black dotted. Figure 5 illustrates the evolution of the injection loss obtained from the GA for different numbers of injected turns. The GA finds a better set of parameters than the previous simulation studies (indicated by the dashed lines[15]). The fact that a longer injection time leads to higher losses also holds for the GA optimization if the available acceptance is filled. However, especially in these cases GA discovers a much better solution. The dependence of the gain factor on the injection loss is of particular interest due to the vacuum degradation problem. In order to define the relationship between

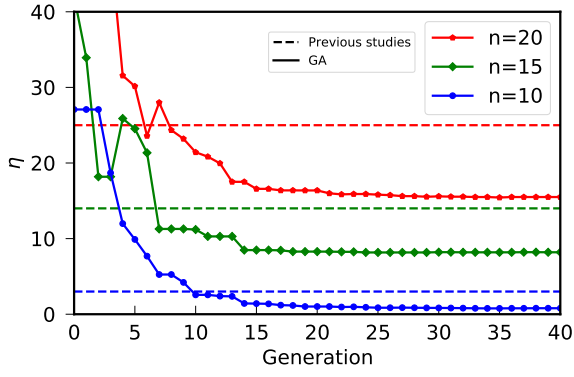

Fig. 5. The evolution of loss for injected emittance of 7 mm · mrad. GA found a much better injection parameter setting for a low loss injection than the previous simulation studies (dashed lines).

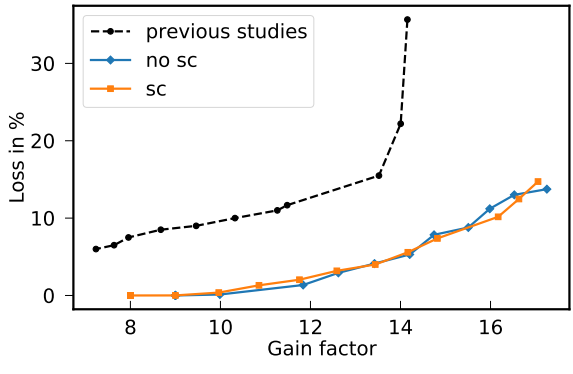

Fig. 6. The PA front for gain factor and MTI loss. GA found a much better PA front than the previous studies.

both, the gain factor has been included as an optimization objective, i.e. to find a 2D Pareto front of both. Figure 6 shows that multi-objectives genetic algorithms (MOGA) finds a much better set of parameters for an improved MTI performance than the previous simulation studies.[15] The influence of space charge on the MTI performance optimization with MOGA is significant even if the discovered PA fronts are similar. The discovered MTI parameters are different with space charge.

For the layout of the injector upgrade and the new proton injector is crucial to known the injection dependence on emittance. The demands on the injector could be relaxed if a sufficient MTI performance with a large injection emittance can be discovered. Previous MTI optimization studies[15,17] clearly demonstrate that the horizontal emittance of the incoming beam has a significant impact on MTI performance. The smaller the injected emittance is, the better the MTI performance gets, which is contradicting to relaxation of the injector demands. A reduction of the horizontal emittance can be achieved e.g. by horizontal collimation[17] or by

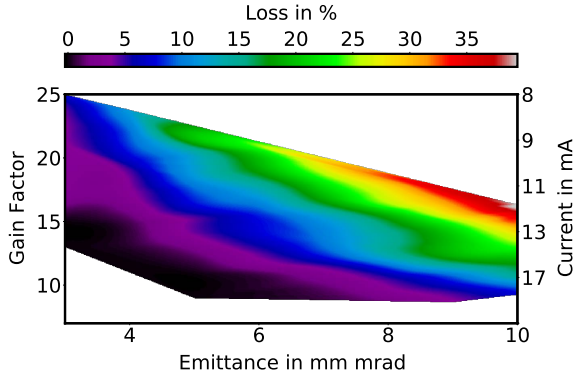

Fig. 7. The 3D Pareto front for a simultaneously GA optimization of gain factor, loss and emittance. On the right axes the require injector current is shown to reach the space charge limit in the SIS18.

a round-to-flat transformation.[16] Figure 7 shows in accordance with MTI model and previous studies the trade-off between the objectives over a wide range of parameter variations, which can be summarized as follows: no loss means small injected emittance and low gain factor; a high gain factor implies small emittance with medium loss; and large emittance means very large loss and small gain factors. This trade-off is a direct consequence of Liouville's theorem. The obtained results for single and double objective optimization are located also on the 3D PA front. Optimization with multi-objective particle swarm (MOPSA) shown similar result with fast convergence. A 3D Pareto front has been generated for proton injector is also shown in Fig. 8.[18] The outcome of this optimization study and heuristic analysis of the MTI demonstrate that a low-loss injection for several emittance over many turns for various proton currents could be achieved. Three case with brilliance of 4, 5 and 6 mA/(mm mrad) has been marked in Fig. 8. With each brilliance, the

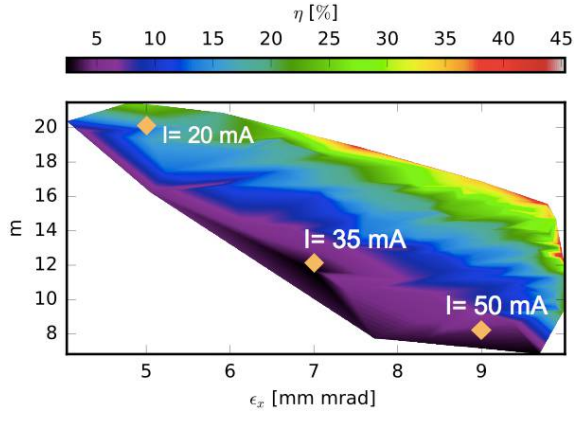

Fig. 8. Proton linac MTI performance plot for the SIS18 synchrotron.

space charge limit in SIS18 can be reached, but the higher plinac brilliance allow a lower loss injection.

4. Online Injection Optimization

At the GSI facility, accelerator setup and readjustment — like the multi-turn injection optimization — is typically done manually and is very time-consuming. With the FAIR project, the complexity of the facility increases furthermore and for efficiency reasons, it is recommended to establish a high level of automation. Modern Accelerator Control Systems allow a fast access to both, accelerator settings and beam diagnostics data. This provides the opportunity to implement evolutionary algorithms for automated adjustment. An end-user application exploiting the genetic algorithm framework Jenetics[19] to optimize unknown beamline settings through the Java-based FAIR control system has been implemented.[20] Jenetics is an end-user ready software library implementing an evolutionary algorithm written in modern day Java. Therefore the choice to use Jenetics was obvious although faster algorithm are known.[11] The end-user application has been carefully tested with the local injector of the CRYRING@ESR. The tests were performed using a 40 keV deuterium beam from the local ion source. The ion source produced an ion beam with a total intensity between 300–800 μA. Almost 90% of this mixture was D_2^+, the remaining 10% was dominated by D^+. The genetic optimizer could find the more intense D_2^+ mass peak detected within a broad parameter range of the mass separation magnet. The performance in terms of transmission and time was comparable

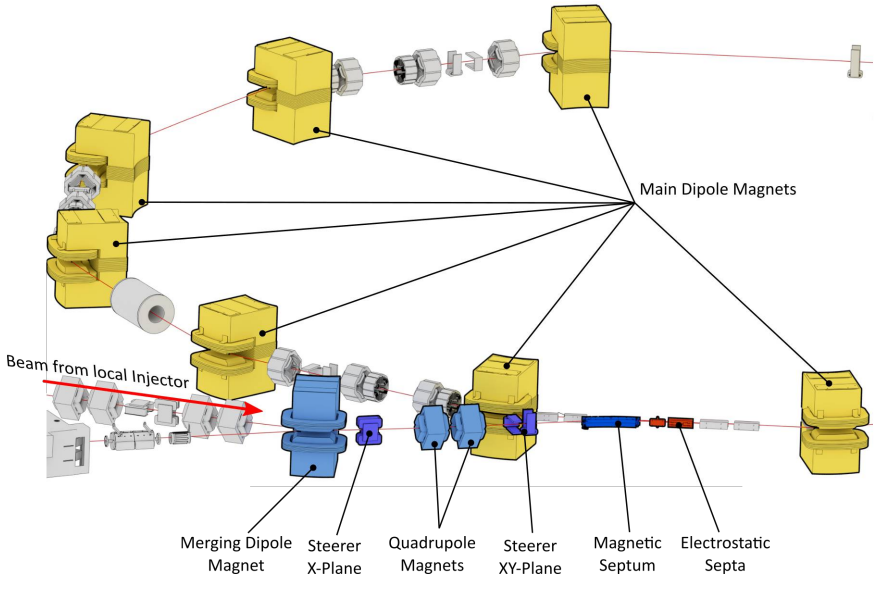

Fig. 9. (Color online) CRYRING@ESR injection. The items emphasized by color were controlled by the genetic algorithm.

to what the standard mass scan revealed. After this successful test, the multi-turn injection of the CRYRING@ESR from the local injector has been optimized online with a genetic algorithm with the aim to maximize the stored beam current. The relative beam current has been measured with the longitudinal Schottky diagnostics in the CRYRING@ESR. The Jenetics algorithm independently controlled 10 parameters (see Fig. 9): the deflection angle of the merging dipole magnet, focusing strengths of two quadrupole magnets and strengths of three steerer in the transfer line as well as the deflection angles of the magnetic septum and two electrostatic septa, and the closed orbit defined by the ring dipoles. The result of the successful evolutionary algorithm optimization performance is presented in Fig. 10. Shown are two cases of converged genetic scans for the recombination probability of 0.5 and 0.8. The population size was 50 and the offspring fraction 0.5. The tournament size of 15 has been chosen rather large to reach a fast convergence. For large tournament size, weak individuals have less chance of being selected. The first population is created randomly forming a range around 10–15% of known good values (e.g. from earlier manual settings or beam optics calculations). The performance of the

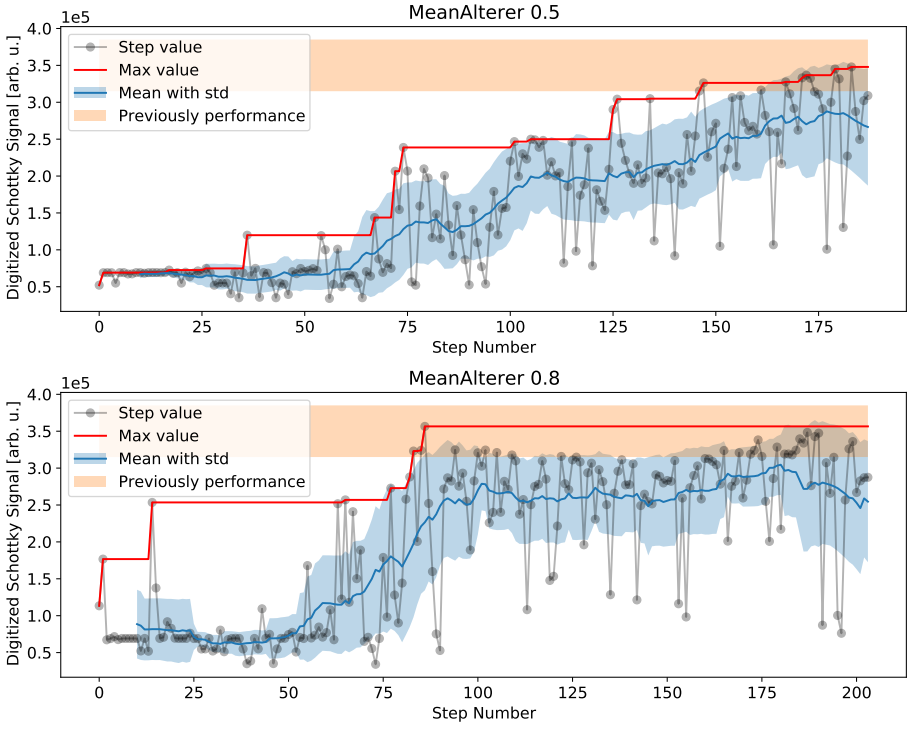

Fig. 10. Converged genetic scan driving ten parameters for two different recombination probability. The goal of the optimization has been to maximize the CRYRING@ESR MTI performance. The scans reached the final value after four generations and reached previous good transmission after 89 (upper scan) and 97 minutes (below scan). For each optimization step an averaging over ten measurements has been performed.

ion source, especially unstable plasma conditions play a crucial role, as it introduces nondeterministic transmission fluctuations which cannot be coped with by the algorithm without further measures. Therefore for each genetic scan step an average of over ten measurements has been performed. Both scans reached previously achieved transmission after about 1.5 hours optimization time. At present, the performance speed is limited by the FAIR control system. Hence, removing performance bottlenecks in the FAIR control system code stack would be a key to fully enable this method's power.

5. Machine Learning

A principal characteristic of Machine Leaning (ML) is to implicitly deduce a set of rules from given data, mapping specific input to output, relieving the user from this tedious task. As such ML is especially suited for problems whose solutions require either a lot of manual fine-tuning or involve long lists of (potentially unknown) rules. Relevant for the presented problem is the latter case, where supervised machine learning consisting of regression models is used to predict continuous variables from the given data. Supervised ML covers many different algorithms with varying complexity, from linear approximations like Linear Regression (LR) up to "biologically inspired" Artificial Neural Networks (ANN).[21]

5.1. *Linear regression*

One of the simplest estimators is the Linear Regressor. Linear regression is a linear approach modeling the relationship between the scalar dependent variable and one or more explanatory variables. In linear regression, the relationship is modeled using linear predictor functions whose unknown model parameters are estimated from the data. The least squares approach is often used for fitting linear regression models. This model has the advantage of being very simple, and is usually a great start when testing a Machine Learning problem. Furthermore, the predictions of this model are usually very fast, as the complexity of the regression is linear.[21]

5.2. *Artificial neural networks*

Artificial neural networks (ANN) are computing systems vaguely inspired by the biological neural networks found in animal brains. The most basic form of ANN typically utilized in supervised learning problems is a fully-connected feed-forward Multi-Layer Perceptron (MLP). It is a specific ANN architecture which is represented by consecutive layers of nodes where all nodes of two consecutive layers are connected to each other. Each node sums all its weighted inputs and transforms the result using an activation function. The activation function should be nonlinear in order to represent nonlinearities in the data and it must be differentiable in order to comply with the fitting procedure. Weights are usually randomly initialized and then iteratively updated during the fitting procedure in order to minimize the selected loss function.

6. IPM Profile Reconstruction

The principle of IPMs is as follows: the primary beam ionizes the residual gas and the ionized particles (ions or electrons) are extracted via electric fields, sometimes in conjunction with magnetic fields to confine the movement of ionized particles in the plane transverse to the electric field.[22] In the ideal case, the ionized particles were moving on straight paths towards the detector and the profile of the extracted particles would then reflect a one-dimensional projection of the transverse profile of the primary beam. The electromagnetic fields of the primary beam can however affect the trajectory of particle movement towards the detector, resulting in a deflection with respect to their original position, see Fig. 11. As a consequence, the measured beam profile can be significantly deformed compared to the actual beam distribution. Due to the complex nature of the corresponding profile transformation, a machine learning-based approach assisted by accurate simulation models of the IPM including beam space-charge effects was performed.

The Virtual-IPM simulation tool was used for simulating the movement of electrons inside the IPM region for a typical LHC case,[23] where the beam electric field leads to major distortion. A total of 21 021 profiles were simulated, with beam parameters randomly sampled from the relevant parameter region (enclosing the region for typical beam parameters). The varied beam parameters are bunch width, bunch height, bunch length and bunch intensity. The simulated profiles were then binned corresponding to the resolution of an acquisition system based on hybrid-pixel detector,[24] resulting in 98 bins per profile. Together with the bunch length and the bunch intensity, this data were used as an input to various regression models. An additional preparation step involved centering and scaling each of the input features to have zero mean and unit standard deviation. In a first attempt, the original beam width, in form of the Gaussian profile standard deviation, was used as the target output. Even the simple linear regression model showed very promising results for this setup.[23] In a subsequent study, a more complex artificial neural network (ANN) was used to reconstruct the complete beam profile shapes as shown

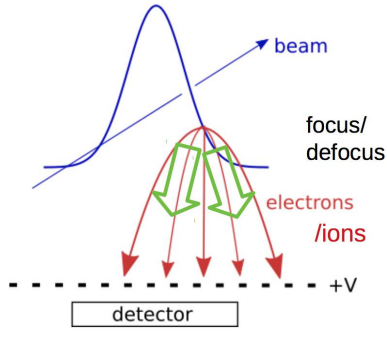

Fig. 11. In the ideal case the ionized particles would move on straight lines towards the detector. However the electromagnetic field of the beam can influence the particle movement as indicated.

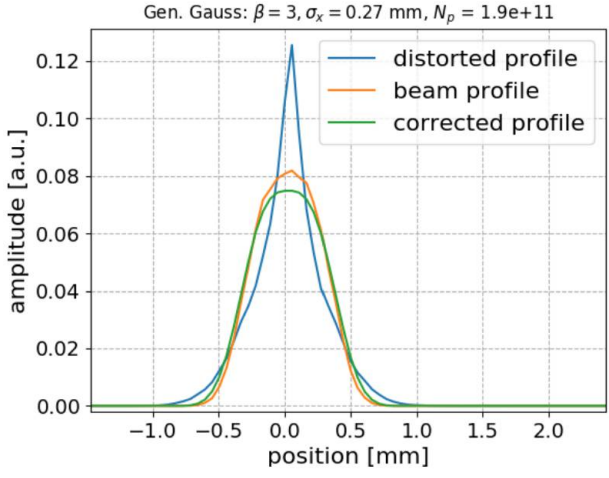

Fig. 12. Simulation of profile distortion due to space-charge using Virtual-IPM together with the ANN corrected profile. The simulated profile is represented by a generalized Gaussian distribution with exponent $\beta = 3$.

in Fig. 12.[25] The ANN consists of two fully connected hidden layers with 88 nodes each, using *tanh* activation, and a fully connected output layer using linear activation which resembles the reconstructed beam profile. The input layer consists of 100 nodes, including 98 profile bins as well as the the bunch length and bunch intensity. Adam optimizer with learning rate 1×10^{-4} was used for fitting together with mean-squared error loss. Fitting converged after about 30 epochs with batch size of 32 samples. Interesting to note is that, though training was performed only with Gaussian profiles, the fitted ANN manages to reconstruct non-Gaussian beam shapes such as generalized Gaussian or Q-Gaussian shapes to a satisfactory degree as well, as depicted in Fig. 12.

7. Conclusion and Outlook

A fast beam dynamics simulation model has been developed and used together with a multi-objective genetic algorithm to optimize the multi-turn injection into SIS18. A loss-free or low-loss injection for several emittance over many turns were identified. Space charge results in a similar PA front, but with different injection settings. With the optimized multi-turn injection a range of injector brilliance could be defined. This crucial information gives more flexibility for the layout of the SIS18 injectors.

An automated online optimization of multi-turn injection into the storage ring CRYRING@ESR has been presented. After 1.5 h of optimization time, best previous transmission could be reached. The nature-inspired optimization has potential to reduce the manpower requirements and variations of quality performance due to the manual procedure. Looking forward, the algorithm shall be applied to SIS18.

A novel method for resolving IPM profile distortion under the influence of magnetic guiding fields based on machine learning has been presented. The first investigations, using simulated data, yield promising results. Next steps include estimation of influence of error sources on predictions, optimization of model selection and application of the method to measured data. The method has a potential to extend usability and reduce cost of IPMs for high brightness beams. The application of machine learning to time-domain signals like the longitudinal Schottky signals is under investigation.

References

1. P. Spiller *et al.*, FAIR Technical Design Report, 2008.
2. E. Mustafin *et al.*, *Nucl. Instrum. Methods A* **510**, 199 (2003).
3. S. Appel *et al.*, *Nucl. Instrum. Methods A* **852**, 73 (2017).
4. S. Reimann *et al.*, Building an operation team for FAIR nearly from scratch, presentation at WAO10, 2016.
5. S. Ratschow *et al.*, The high energy beam transport system for FAIR, in *Proc. EPAC08* (Genoa, Italy, 2008), pp. 3608–3610.
6. F. Herfurth *et al.*, Commissioning of the low energy storage ring facility CRYRING@ESR, in *Proc. 11th Workshop on Beam Cooling and Related Topics (COOL'17)* (Bonn, Germany, 2017), pp. 81–83.
7. W. Geithner *et al.*, *Hyperfine Interact.* **238**, 13 (2017).
8. O. Gorda *et al.*, *Phys. Scr.* **T166**, 14043 (2015).
9. A. Källberg and A. Simonsson, Beam steering with image processing in the CRYRING injection beamline, in *Proc. DIPAC'99* (Checster, UK, 1999), pp. 118–119.
10. A. Konak, D. W. Coit and A. E. Smith, *Reliab. Eng. Syst. Saf.* **91**, 992 (2006).
11. X. Pang and L. Rybarcyk, *Nucl. Instrum. Methods A* **741**, 124 (2013).
12. L. Groening *et al.*, Upgrade of the universal linear accelerator UNILAC for FAIR, in *Proc. 7th Int. Particle Accelerator Conf. (IPAC'16)* (Busan, Korea, 2016), pp. 880–882.
13. F. Fortin and D. Rainville, *J. Mach. Learn. Res.* **13**, 2171 (2012), https://github.com/DEAP/deap.
14. A. Shishlo *et al.*, *Procedia Comput. Sci.* **51**, 1272 (2015), doi:10.1016/j.procs.2015.05.312, https://github.com/PyORBIT-Collaboration.
15. S. Appel, O. Boine-Frankenheim, Multi-turn injection into a heavy-ion synchrotron in the presence of space charge, arXiv:1403.5972v1.
16. S. Appel *et al.*, *Nucl. Instrum. Methods A* **866**, 36 (2017).
17. Y. El-Hayek *et al.*, Initial beam loss and control of dynamic vacuum effects in SIS18, in *Proc. IPAC'13* (Shanghai, China, 2013), pp. 300–302.
18. C. Kleffner *et al.*, Status of the FAIR Proton Linac, in *Proc. LINAC'18* (Beijing, China, 2018), pp. 787–789.
19. F. Wilhelmstötter, Jenetics advanced genetic algorithm, http://jenetics.io.
20. W. Geithner *et al.*, Genetic algorithms for machine optimization in the FAIR control system environment, in *Proc. IPAC'18* (Vancouver, Canada, 2018), pp. 4712–4715.
21. A. Géron, *Hands-On Machine Learning with Scikit-Learn and TensorFlow* (O'Reilly, 2017).
22. R. Singh, M. Sapinski and D. M. Vilsmeier, Simulation supported profile reconstruction with machine learning, in *Proc. 6th Int. Beam Instrumentation Conf. (IBIC'17)* (Grand Rapids, MI, USA, 2017), pp. 350–354.

23. D. Vilsmeier *et al.*, Reconstructing Space-charge distorted IPM profiles with machine learning algorithms, in *Proc. IPAC'18* (Vancouver, BC, Canada, 2018), pp. 2099–2102.
24. S. Levasseur *et al.*, Time-Resolved transverse beam profile measurements with a rest gas ionisation profile monitor based on hybrid pixel detectors, in *Proc. IPAC'18* (Vancouver, BC, Canada, 2018), pp. 2361–2364.
25. M. Sapinski *et al.*, Application of machine learning for the IPM-based profile reconstruction, in *Proc. HB'18* (Daejeon, Korea, 2018), pp. 410–415.